Cellular Physiology and Biochemistry

Cell Physiol Biochem 2018;51:1544-1565
DOI: 10.1159/000495645
Published online: 29 November 2018
Accepted: 21 November 2018

Original Paper

Spatial Relationship and Functional Relevance of Three Lipid Domain Populations at the Erythrocyte Surface

Louise Conrard[a] Amaury Stommen[a] Anne-Sophie Cloos[a] Jan Steinkühler[b] Rumiana Dimova[b] Hélène Pollet[a] Donatienne Tyteca[a]

[a]CELL Unit, de Duve Institute & Université catholique de Louvain, Brussels, Belgium, [b]Theory and Bio-Systems, Max Planck Institute of Colloids and Interfaces, Science Park Golm, Potsdam, Germany

Key Words
Fluorescence microscopy • Mechanical stimulation • Piezo1 • PMCA • PDMS stretching • Calcium exchanges

Abstract
Background/Aims: Red blood cells (RBC) have been shown to exhibit stable submicrometric lipid domains enriched in cholesterol (chol), sphingomyelin (SM), phosphatidylcholine (PC) or ganglioside GM1, which represent the four main lipid classes of their outer plasma membrane leaflet. However, whether those lipid domains co-exist at the RBC surface or are spatially related and whether and how they are subjected to reorganization upon RBC deformation are not known. ***Methods:*** Using fluorescence and/or confocal microscopy and well-validated probes, we compared these four lipid-enriched domains for their abundance, curvature association, lipid order, temperature dependence, spatial dissociation and sensitivity to RBC mechanical stimulation. ***Results:*** Our data suggest that three populations of lipid domains with decreasing abundance coexist at the RBC surface: (i) chol-enriched ones, associated with RBC high curvature areas; (ii) GM1/PC/chol-enriched ones, present in low curvature areas; and (iii) SM/PC/chol-enriched ones, also found in low curvature areas. Whereas chol-enriched domains gather in increased curvature areas upon RBC deformation, low curvature-associated lipid domains increase in abundance either upon calcium influx during RBC deformation (GM1/PC/chol-enriched domains) or upon secondary calcium efflux during RBC shape restoration (SM/PC/chol-enriched domains). Hence, abrogation of these two domain populations is accompanied by a strong impairment of the intracellular calcium balance. ***Conclusion:*** Lipid domains could contribute to calcium influx and efflux by controlling the membrane distribution and/or the activity of the mechano-activated ion channel Piezo1 and the calcium pump PMCA. Whether this results from lipid domain biophysical properties, the strength of their anchorage to the underlying cytoskeleton and/or their correspondence with inner plasma membrane leaflet lipids remains to be demonstrated.

Donatienne Tyteca

CELL Unit, de Duve Institute & Université catholique de Louvain,
UCL B1.75.05, avenue Hippocrate, 75, B-1200 Brussels (Belgium)
Tel. +32-2-764.75.91, Fax +32-2-764.75.43, E-Mail donatienne.tyteca@uclouvain.be

Introduction

Red blood cells (RBCs) are highly deformable cells that can go through capillaries 3-times narrower than their diameter to deliver oxygen throughout the body. The RBC deformation process is associated with a transient increase of the intracellular calcium [1] which plays a capital role, notably by activating Gardos channels and thus leading to cell dehydration, and by favoring a local uncoupling between the membrane and the underlying spectrin cytoskeleton [2]. RBC calcium entry is thought to be mostly operated by mechano-activated ion channels like Piezo1 [3], while calcium efflux is ensured by the RBC calcium pump, the Plasma Membrane Calcium ATPase (PMCA). This process is tightly regulated and an excessive increase of the intracellular calcium, as observed in physiological senescence or in pathological hereditary hemolytic anemias, has harmful consequences for the RBCs such as an increased vesiculation, the loss of the transverse lipid asymmetry and the consumption of the energy resources. This will lead to a decreased deformability resulting in the RBCs trapping in the spleen and their removal from the blood by the spleen resident macrophages [4].

Besides finely regulated calcium exchanges, RBC deformability has also been linked to other specific features, *i.e.* (i) the excess of plasma membrane (PM) surface in comparison with the cytoplasmic volume and the resultant biconcave shape; (ii) the tightly regulated intracellular hemoglobin concentration (32-36 g/dl); and (iii) the viscoelastic resistance of the membrane [5, 6]. The latter feature depends on the strong anchorage of the PM to a very stable cytoskeleton of spectrin thanks to two non-redundant anchorage complexes based on 4.1R and ankyrin proteins [7]. Membrane lipid composition is also suggested to regulate the membrane viscoelastic properties [8]. As a matter of fact, RBC PM exhibits a particularly high cholesterol level (~45 mol%) in comparison to other cell types (*e.g.* ~35 mol% in CHO cells or ~15 mol% in fibroblasts) [9]. Yet, this small lipid plays key roles in membrane by regulating fluidity, lipid phase separation, mechanic resistance and membrane permeability [10].

As the scientific community slowly realized the importance of membrane lipid composition for cell biological characteristics and processes, more and more evidences for lateral lipid asymmetric distribution have been provided. The first example was the well-known 'lipid rafts', defined as nanometric and transient lipid structures whose presence has been linked to several processes like lipid sorting in polarized cells and antigen presentation at the T-cell surface [11, 12]. In the last decades, advances in microscopy resolution and development of new observation techniques (*e.g.* super resolution microscopy or fluorescence lifetime spectroscopy) [13-16] and more relevant lipid probes [17, 18] have allowed to evidence bigger (submicrometric instead of nanometric) and more stable lipid domains. Those have been observed on prokaryotic cells [19], yeast [20, 21] and various eukaryotic cells like keratinocytes [22], fibroblasts [23] and RBCs [24-26]. Focus is generally made on sphingolipids and sterols as they are two major lipids of the PM external leaflet of many cells and because they are known to be enriched in rafts and associated with membrane fluidity regulation.

As a matter of fact, our group evidenced and extensively characterized cholesterol (chol)- and sphingomyelin (SM)-enriched submicrometric domains at the external PM leaflet of RBCs. These domains are stable in time and space and have been observed by fluorescence microscopy on RBCs immobilized on poly-L-lysine (PLL, *i.e.* spread), but also on RBCs in suspension in plastic chambers or in three-dimensional gels. To label the domains for fluorescence microscopy, we used fluorescent lipid analogs (*i.e.* BODIPY-SM) that get inserted at trace levels in the PM [27] and developed and carefully validated fluorescent toxin fragments specific to endogenous chol (theta*) and SM (lysenin*) [25, 26]. More recently, we also used atomic force microscopy, a high-resolution technique applicable to cells in their native state (*i.e.* without labeling), to study the biophysical properties of these domains [28]. The chol- and SM-enriched domains differ in abundance and biophysical properties (*i.e.* lipid order and association with membrane curvature areas) and differentially contribute to the

RBC deformation. For instance, chol-enriched domains gather in high-curvature membrane areas under RBC stretching and might thus increase deformability and membrane resistance under deformation; while SM-enriched domains, which increase in abundance after deformation, could be linked to RBC shape restoration after deformation [29].

Lipid domains enriched in phosphatidylcholine (PC) or glycosphingolipids like ganglioside GM1 have also been evidenced but not well-characterized [27]. Moreover, whether chol-, SM-, PC- or GM1-enriched domains coexist or are spatially related at the RBC surface and whether they are subjected to reorganization upon RBC deformation are not known. We explored the first issue on RBCs at resting state. Since multiple labeling could suffer from the use of several probes at the same time, possibly inducing toxicity and steric hindrance, we developed additional approaches aiming at comparing lipid domains for their abundance, biophysical properties (lipid order and curvature association, key properties involved in cell deformation) and ability to be modulated by temperature and controlled chol depletion. We next studied lipid domain organization through RBC deformation by mechanically stimulating RBCs (using stretchable silicon chambers) and modulating either the entry or the exit of calcium.

The present study shows the coexistence at the resting RBC PM outer leaflet of three lipid domain populations that differ in chol-, SM-, PC- and GM1-enrichment, abundance, curvature association, lipid order, temperature dependence and sensitivity to RBC spreading onto PLL. Regarding lipid domain contribution to RBC reshaping, we have previously shown that the first population of domains, *i.e.* those mostly enriched in chol, gather in increased curvature areas upon RBC deformation [29]. Here, we provide experimental evidence for the differential contribution of the two other populations of lipid domains in RBC calcium exchanges. This could occur either via the mechano-activated ion channel Piezo1 during deformation or via the calcium pump PMCA during shape restoration.

Materials and Methods

Red blood cell isolation

This study was approved by the Medical Ethics Committee of the Université Catholique de Louvain; each donor gave written informed consent. All methods were performed in accordance with the relevant guidelines and regulations. Blood was collected from 10 healthy volunteers by venopuncture into dry K^+/EDTA-coated tubes. For each experiment, blood was diluted 1:10 in Dulbecco's Modified Eagle Medium (DMEM containing 25 mM glucose, 25 mM HEPES and no phenol red, Invitrogen), then washed twice by centrifugation at 200 *g* for 2 min and resuspension. Washed RBCs were used at 5 * 10^7 cells/ml (washed RBCs:medium ratio of 1:10, *v:v*), then incubated or not with pharmacological agents or directly imaged by vital fluorescence/confocal microscopy or fluorescence correlation spectroscopy (FCS) (see below).

Pharmacological treatments

To modulate chol content, washed RBCs were preincubated in suspension at 37°C in DMEM supplemented with (i) the indicated concentrations of methyl-ß-cyclodextrin (mβCD; Sigma-Aldrich) for 30 min or (ii) 0.9 mM mβCD followed by repletion with 3.5 µg/ml mβCD:chol (Sigma-Aldrich) for 60 min. Chol content was determined as previously described [25]. SM content modulation was achieved with sphingomyelinase from *Bacillus Cereus* (Sigma-Aldrich) as described in [26]. To inhibit mechano-activated channels, labeled and immobilized RBCs were incubated with 7 µM GsMTx4 peptide (Abcam) for 15 min and observed upon treatment maintenance. To activate Piezo1 channels, labeled and immobilized RBCs were incubated with 0.5 µM Yoda1 (Biotechne) for 20 sec, washed and directly observed. To activate protein kinase C (PKC), RBCs were pre-incubated with 6 µM phorbol 12-myristate 13-acetate (PMA, Sigma-Aldrich) and 20 nM Calyculin A from Discodermia Calyx (CalA, Sigma-Aldrich) for 15 min at 37°C before labeling (upon maintenance of PMA/CalA treatment). To modulate calcium content, RBCs were pre-incubated in calcium-free homemade medium containing 1 mM calcium-chelating agent ethylene glycol-bis(β-aminoethyl ether)-N,N,N',N'-tetraacetic acid (EGTA, Sigma-Aldrich) for 10 min at RT before labeling (upon maintenance of EGTA). Residual calcium content was assessed as described below. RBCs were then possibly incubated

in 1.8 mM calcium-containing medium for 20 min to achieve calcium repletion. To modulate ATP content, RBCs were pre-incubated in glucose-free homemade medium for 2 h at 37°C before labeling. Residual ATP content was assessed by a luminescent ATP detection assay kit (Abcam). RBCs were then possibly incubated in 25 mM glucose-containing medium for 30 min to achieve glucose repletion. Treatment innocuity has been assessed by measuring the percentage of hemoglobin release (absorbance at 450 nm).

Vital fluorescence/confocal imaging

To immobilize RBCs for imaging, two complementary systems were used: RBCs spread onto poly-L-lysine (PLL, 70–150 kDa; Sigma-Aldrich)-coated coverslips and RBCs in suspension. For spread RBCs, coverslips were first coated with PLL:DMEM (1:1, *v:v*) at 37°C for 40 min, then washed with DMEM at 20°C for 5 min. Labeled RBCs were then dropped onto the coated coverslips at 20°C for exactly 4 min, the suspension was removed and replaced by fresh medium, and attached RBCs were allowed to spread for another 4 min. The coverslip was placed upside down on a Lab-Tek chamber and then observed. For the "in suspension" system, labeled RBCs were dropped to settle down in µ-Slide VI0.4 uncoated IBIDI chambers (IBIDI, Proxylab; 100 µl by channel). All preparations were examined at the labeling temperatures, either with a Zeiss LSM510 confocal/multiphoton microscope using a plan-Apochromat 63X NA 1.4 oil immersion objective or with a Zeiss wide-field fluorescence microscope (Observer.Z1) using a plan-Apochromat 100X/1.4 oil Ph3 objective.

Decoration of endogenous lipids by toxin fragments and fluorescent lipid insertion*

Washed RBCs were labeled with toxin* fragments, BODIPY-lipids (SM, PC, GM1) or TopFluor-TMR-PC. Lysenin* and theta* were produced as previously described [25, 26], dissolved in 1 mg/ml DMEM-BSA (Bovine Serum Albumin, Sigma) and cleared of aggregates before each experiment by centrifugation at 20, 000 *g* for 10 min. RBC labeling with toxins* was performed in suspension (*i.e.* before immobilization) with either 1.25 µM lysenin* or 0.55 µM theta* in DMEM/BSA at the indicated temperatures for 25 min under continuous agitation, then pelleted at 200 *g* for 2 min and resuspended in DMEM. RBC labeling with 0.6 µM BODIPY FL C5-SM, 1 µM BODIPY FL C5-GM1 or 1 µM BODIPY FL C5-HPC (Invitrogen) and 0.8 µM TopFluor-TMR-PC (Avanti polar lipids) was performed after RBC immobilization on coverslips at the indicated temperatures for 15 min. For co-labeling, RBCs were either labeled in suspension with toxin* fragments, immobilized and then labeled with fluorescent lipid analogs, or directly immobilized and co-labeled with fluorescent lipid analogs.

Lipid order

A stock solution of 2-dimethylamino-6-lauroylnaphthalene (Laurdan) was prepared in dimethyl sulfoxide (DMSO) and conserved as described in [30]. Washed RBCs were labeled at RT in suspension in DMEM/BSA containing 2.5 µM Laurdan for 60 min. 1.25 µM lysenin*, 0.55 µM theta* or 0.8 µM TopFluor-TMR-PC were added for the last 20 min. RBCs were then immobilized and examined using (i) confocal mode for lipids and (ii) multiphoton mode with acquisition at 440 nm and 490 nm and a Normaski prism for Laurdan. Lipid order determination was performed as described in [30] and in [31]. Briefly, domains and surrounding membrane ROIs and masks were obtained from the two fluorescent channels (440 nm and 490 nm) of Laurdan images. The determination of Laurdan domains co-localizing or not with the lipid domains and the following separation of the domain masks were done manually by comparing Laurdan and lipid images. A 2D GP map, where GP for each pixel were calculated from a ratio of the two fluorescence channels, was created from those masks using MATLAB (The MathWorks, Natick, MA). Briefly, each image was binned (2 × 2) and thresholded, then the GP image was calculated for each pixel using the GP equation as described in [30], and the G factor was measured as recommended in [30].

Fluorescence correlation spectroscopy

RBCs were immobilized on coverslips and labeled with 1 µM BODIPY-GM1 (as described above) and 25 nM FAST DiI (1, 1'-Dilinoleyl-3, 3,3',3'-Tetramethylindocarbocyanine, 4-Chlorobenzenesulfonate), then examined at RT on confocal microscope Leica TCS SP5 (Wetzlar, Germany) with a 63X 1.2 NA water immersion objective and 1 Airy unit. FAST DiI was excited using a 561 solid state laser and emission was collected between 607 nm and 683 nm using a filter cube. To check for bleed-through artifacts, RBCs were labeled with BODIPY-GM1 alone and in this case no significant signal was detected. The intersection

between confocal volume and RBC membrane was adjusted to the maximum photon count and positioned either on a membrane domain or a segment of the membrane exhibiting homogenous fluorescence. Photon counting was accomplished by avalanche photodiodes (Leica, Wetzlar, Germany) and time correlations were calculated at a sampling frequency of 200 kHz for a time interval of 30 sec. Each measurement point was repeated for three consecutive measurements. The obtained correlation curves were fitted using a 1-component 2D diffusion model: $G(\tau) = \frac{1}{<N>} \frac{1}{\left(1+\frac{\tau}{\tau_0^2}\right)}$

Here, τ_0 is the average residence time inside the intersection of the confocal volume and <*N*> is the average number of fluorophores in the detection volume. Only correlation traces with a satisfying fit to the model ($R^2 > 0.98$) were considered in the analysis.

RBC (de)stretching on PDMS chambers

Deformation experiments were conducted by spreading BODIPY-SM-, GM1- or Fluo-4 (see below)-prelabeled RBCs on a 4 cm^3 polydimethylsiloxane (PDMS) stretchable chamber (Strex Inc). Briefly, PDMS chambers were coated with PLL:DMEM (1:1, *v:v*) at 37°C for 40 min, washed with DMEM at 20°C for 5 min and fixed to the stretching device (STREX, cell strain instrument, B-Bridge). Labeled RBCs were plated into the PDMS chamber for exactly 5 min, then the suspension was removed and replaced by fresh medium, and attached RBCs were allowed to spread for another 5 min. The PDMS chamber was then immediately observed at RT without stretching (unstretched) with a Zeiss wide-field fluorescence microscope (Observer. Z1) using a plan-Neofluar 63X/0.75 Ph2 objective. Stretching and destretching of the chamber were thereafter respectively performed by (i) quick (1 min) axial stretching of the right side of the PDMS chamber of 12 % of the chamber length (stretching); and (ii) return to the initial state (destretching).

Medium osmolarity modulation

CellASIC ONIX Microfluidic platform (Merck Millipore) has been used to achieve real-time imaging on living RBCs. The following media were disposed each in a well and allowed to flow successively to the central chamber: PLL (15 min, low flow), DMEM (5 min, medium flow), washed RBCs (4 min, high flow), DMEM (10 min, medium flow), toxin* or fluorescent lipid analog (15 min, low flow), DMEM (3 min, medium flow), hypo-osmolar medium (180 mOsm, 10 min, low flow). Images were acquired every 45 sec using a Zeiss LSM510 confocal microscope.

Calcium labeling and measurement

To label intracellular calcium, washed RBCs were incubated in suspension at 37°C with 3 µM Fluo-4 acetoxymethyl ester (Fluo-4 AM, Invitrogen) in 1.8 mM calcium-containing homemade medium for 60 min under continuous agitation, pelleted at 200 *g* for 2 min and resuspended in homemade medium, then let for 30 min at 37°C under agitation to allow the Fluo-4AM de-esterification. Fluo-4-labeled cells were then either immobilized, imaged with a Zeiss wide-field fluorescence microscope and analyzed as explained below; or measured in a 96-well plate with a spectrofluorimeter (SpectraCountTM, Packard BioScience Co.) at Exc/Em 490/520 nm and analyzed using hemoglobin content for normalization. As the Fluo-4 fluorescence signal is not a linear function of the calcium concentration [32], only qualitative observations could be made.

Image analysis and data quantification

Lipid domain abundance, curvature association and colocalisation were assessed by manual counting on images from confocal or epifluorescence high-resolution microscope. Measurement of RBC projected area (referred as hemi-RBC area) and Fluo-4 quantification on images was performed using ImageJ software on images where the RBC projected contours have been manually drawn on the transmission images.

Statistical analyses

*V*lues are presented as means ± SEM. Statistical significance was tested either with two-sample t-test or one-way ANOVA followed by Tukey's post-hoc test (NS, not significant; * $p < 0.05$; ** $p < 0.01$ and *** $p < 0.001$).

Results

Polar lipid- and chol-enriched domains differ in abundance, curvature association and lipid order

We have previously shown that chol- and SM-enriched domains differ in abundance [25, 26] and preferentially associate with high and low curvature areas of the biconcave RBC membrane [29]. This analysis was limited to chol and SM while not considering PC, another abundant class of outer PM leaflet lipids, or glycosphingolipids, known to play key pathophysiological roles. Here, we questioned whether PC and GM1 could also participate to the formation of domains at the outer PM leaflet and whether they differ in abundance, curvature association and lipid order as compared to chol- and SM-enriched domains. To these aims, as fluorescent probes, we used (i) theta* toxin to decorate endogenous chol [25]; (ii) lysenin* toxin or PM trace insertion of BODIPY-SM to reveal SM [26]; (iii) PM trace insertion of BODIPY-PC [27] or TopFluor-TMR-PC, two PC analogs that evidence lipid domains of comparable size, shape, localization at the center of spread RBCs (Suppl. Fig. 1A - For all supplemental material see www.karger.com/10.1159/000495645/) and abundance (Suppl. Fig. 1B) and that perfectly co-localize (Suppl. Fig. 1C); and (iv) PM trace insertion of BODIPY-GM1, as in [33].

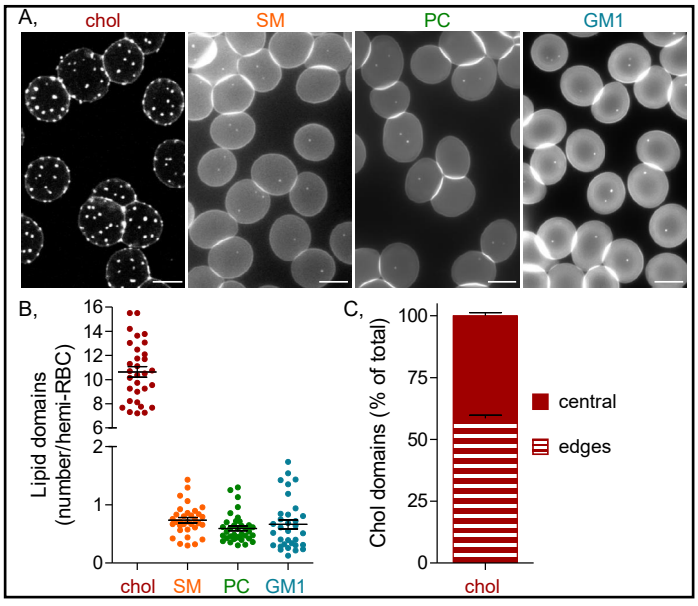

Fig. 1. Unlike polar lipid (SM, PC, GM1)-enriched domains, chol-enriched domains are abundant and equally associate with the center and the edges of spread RBCs. (A) Representative confocal/fluorescence imaging of PLL-spread RBCs labeled with theta* (chol), BODIPY-SM, -PC or –GM1 and examined at 20°C. Scale bars 5 µm. (B) Quantification of lipid domains per hemi-RBC. Means ± SEM from 31-37 experiments, each dot representing one experiment in which >100 RBCs were counted. (C) Distribution of chol-enriched domains between the edges (stripped) and the center of the membrane (full) on spread RBCs. Means ± SEM of 4 independent experiments where >70 RBCs were analyzed.

As shown in Fig. 1A, insertion of BODIPY-PC or -GM1 also revealed well-defined round lipid domains on spread RBCs. These domains exhibited similar abundance as SM-enriched domains but were quite less abundant than those enriched in chol (green and blue dots, respectively, *vs* orange or red dots, Fig. 1B). Moreover, as SM-enriched domains and ~40 % of chol-enriched domains (pictures in Fig. 1A and quantification in Fig. 1C), those enriched in PC and GM1 seemed restricted to the central area of spread RBC membrane (defined as in [29]).

Since RBC spreading can impair RBC biconcavity, we also explored lipid domain topography using plastic chambers compatible with confocal microscopy (IBIDI chambers) as an alternative imaging system in which RBCs were laid down, resulting in suspended, non-spread RBCs (Fig. 2A). This technique allowed to observe alternating regions of high curvature (HC) at the edges of the RBCs and of low curvature (LC) at the center of the cell [29]. We showed that PC- and GM1-enriched domains were preferentially associated with the LC areas of the RBC, like SM-enriched domains (green, blue and orange arrowheads, Fig. 2A), while chol-enriched domains were preferentially located in HC areas (red arrows, Fig. 2A, [29]).

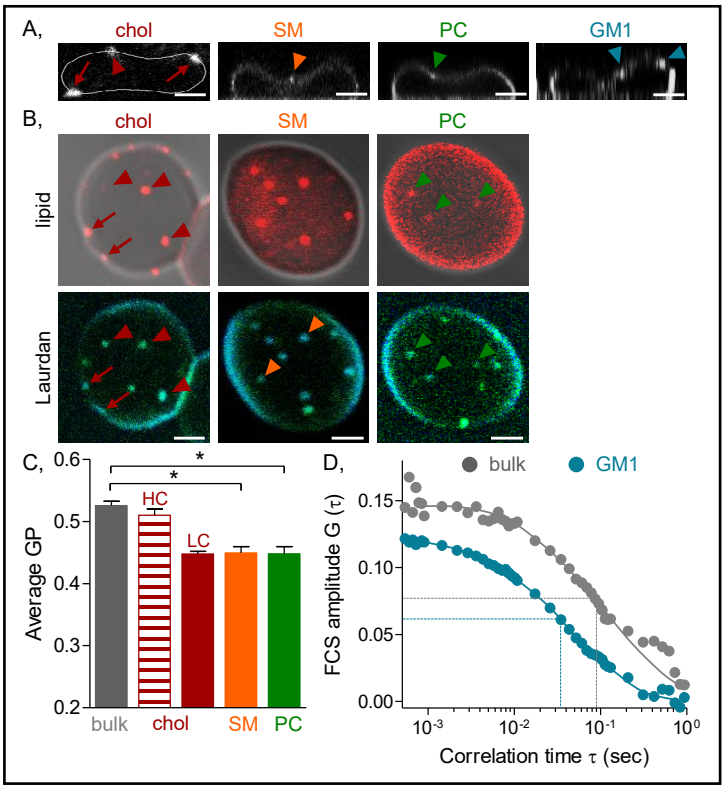

Fig. 2. Unlike polar lipid-enriched domains, chol-enriched domains associate with both low and high curvature areas of suspended RBCs and present differential lipid order. (A) Representative imaging of chol-, SM-, PC- and GM1-enriched domains on RBCs in suspension. RBCs were labeled at 20°C, put in IBIDI chambers and analyzed by confocal imaging. Images shown are reconstruction of Z-stacks and are representative of >2 experiments. (B, C) Membrane lipid order of chol-, SM- and PC-enriched domains determined by Laurdan. (B) RBCs double-labeled at 20°C with theta*, lysenin* or Top-Fluor-TMR-PC (top images) and the fluidity-sensitive probe Laurdan (bottom images) were spread and observed in confocal/biphoton microscopy. Red arrows point to high-curvature chol/Laurdan-enriched domains while red, orange and green arrowheads point to low-curvature lipid/Laurdan-enriched domains. (C) Generalized polarization (GP; proportional to membrane lipid order) of membrane without domains (bulk, grey bar) vs chol-enriched domains sorted according to their curvature localization (HC: high-curvature domains, stripped bar; LC: low-curvature domains, full bar) and polar lipid-enriched domains (orange and green bars). Means ± SEM of 2-3 independent experiments where >100 RBCs have been analyzed. Red and orange bars were reproduced from [31] to facilitate comparison with PC-enriched domains (green bar). (D) Diffusion in GM1-enriched domains determined by FCS. Example of a FCS curve of diffusion in GM1-enriched domains (blue dots) or in the surrounding membrane (grey dots) at 20°C. Time required to decrease the correlation amplitude by half in the studied spot is inversely proportional to the lipid diffusivity. Representative graph of 9 RBCs. All scale bars 2 µm.

Next, we examined whether these different lipid domains could exhibit a differential lipid order by using Laurdan (2-dimethylamino-6-lauroylnaphthalene), an artificial fluorescent probe known for its spectroscopic properties influenced by both the composition and dynamics of its local surrounding [34, 35]. Laurdan allowed us to reveal both the surrounding membrane and submicrometric domains. Hence, each class of lipid domains was recognized by co-labeling between a specific red fluorescent probe and Laurdan. We observed that the vast majority of chol-, SM- and PC-enriched domains in LC areas was marked by Laurdan (red, orange and green arrowheads, Fig. 2B) while only a part of chol-enriched domains in HC was labeled (red arrows, Fig. 2B), in agreement with our previous study [31]. Thanks to the Laurdan fluorescence emission at two wavelengths, we next calculated the Generalized Polarization (GP, see material and methods; proportional to the membrane lipid order) of the chol-, SM- and PC-enriched domains. As previously observed, chol-enriched domains located in HC exhibited a higher lipid order than those present in LC areas (compare stripped to full red columns, Fig. 2C) [31]. On the other hand, all the polar lipid-enriched domains in LC, including those enriched in PC, exhibited a lower lipid order than the surrounding membrane (compare colored columns to the grey column, Fig. 2C). These results indicate that, while lipid domains presented a differential lipid order based on their curvature area association,

those associated with LC cannot be discriminated by this criteria. As the only commercially-available, vital imaging-compatible, monomeric probe for GM1 has an emission wavelength similar to Laurdan, it was impossible to study GM1-enriched domain lipid order by this method. We therefore used Fluorescence Correlation Spectroscopy (FCS) to circumvent this difficulty and explored the diffusion properties of the dye FAST DiI in GM1-enriched domains or in the surrounding membrane (blue dots *vs* grey dots, Fig. 2D). Over 11 analyzed RBCs, 9 had a mean ratio between the diffusion time of GM1-enriched domains and the surrounding membrane of 0.53±0.12, indicating that the dye diffused twice faster in GM1-enriched domains than in the surrounding membrane. The other 2 RBCs had a mean ratio of 2.49±1.09 and exhibited thus domains in which the dye diffused more than twice slower than in the rest of the membrane. This opposite behavior might be explained by the co-existence of two distinct GM1-enriched domain populations or by the presence of lipid domains starting to vesiculate. Even if FCS does not measure the exact same membrane properties as Laurdan, these results seemed in agreement with the hypothesis that most submicrometric polar lipid domains exhibit a lower lipid order than the surrounding membrane. Such observation is in opposition with the general idea that lipid domains are more ordered than the membrane bulk. This could result from the high chol content and the strong membrane:cytoskeleton anchorage found in RBCs.

Altogether, these data suggest that at least two distinct lipid domain populations coexist at the outer PM leaflet of RBCs: those located in HC areas, exhibiting a similar lipid order than the surrounding membrane and mainly enriched in chol, *vs* those located in LC areas with a lower lipid order and enriched in polar lipids and/or chol.

Polar lipid-enriched domains depend on chol for their formation and maintenance

To next explore whether LC domains were co-enriched in polar lipids and chol, we performed double labeling with BODIPY-polar lipids and theta* on spread RBCs (Fig. 3). ~25 % of chol-enriched domains colocalized with polar lipids (yellow arrowheads in Fig. 3A and yellow portions of red columns, Fig. 3B). Considering that RBCs without any polar lipid-enriched domain were excluded from this quantification, this proportion and the lipid domain distribution in LC *vs* HC were in agreement with the simple labeling presented in Fig. 1, excluding artefactual redistribution upon double labeling. In addition, most polar lipid domains were also enriched in chol: ~65 % for SM- and ~85 % for PC- and GM1-enriched domains (yellow portions of

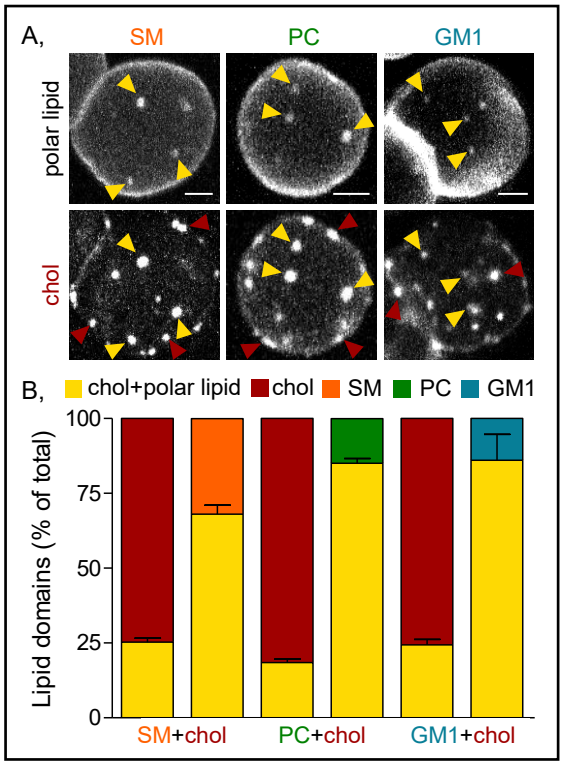

Fig. 3. The majority of lipid domains in low curvature areas are co-enriched in chol and polar lipids. (A) Representative images of PLL-spread RBCs double-labeled at 20°C for polar lipids (top images) and chol (bottom images). Yellow arrowheads point to lipid domains co-enriched in chol and polar lipid, while red arrowheads show domains mainly enriched in chol. Scale bars 2 µm. (B) Quantification. Percentages of chol-enriched domains that colocalize with polar lipid-enriched domains are shown as yellow portions of the red columns. Percentages of polar lipid-enriched domains that colocalize with chol-enriched domains are shown as yellow portions of orange, green or blue columns. Means ± SEM of 2 independent experiments where 24-38 RBCs were analyzed.

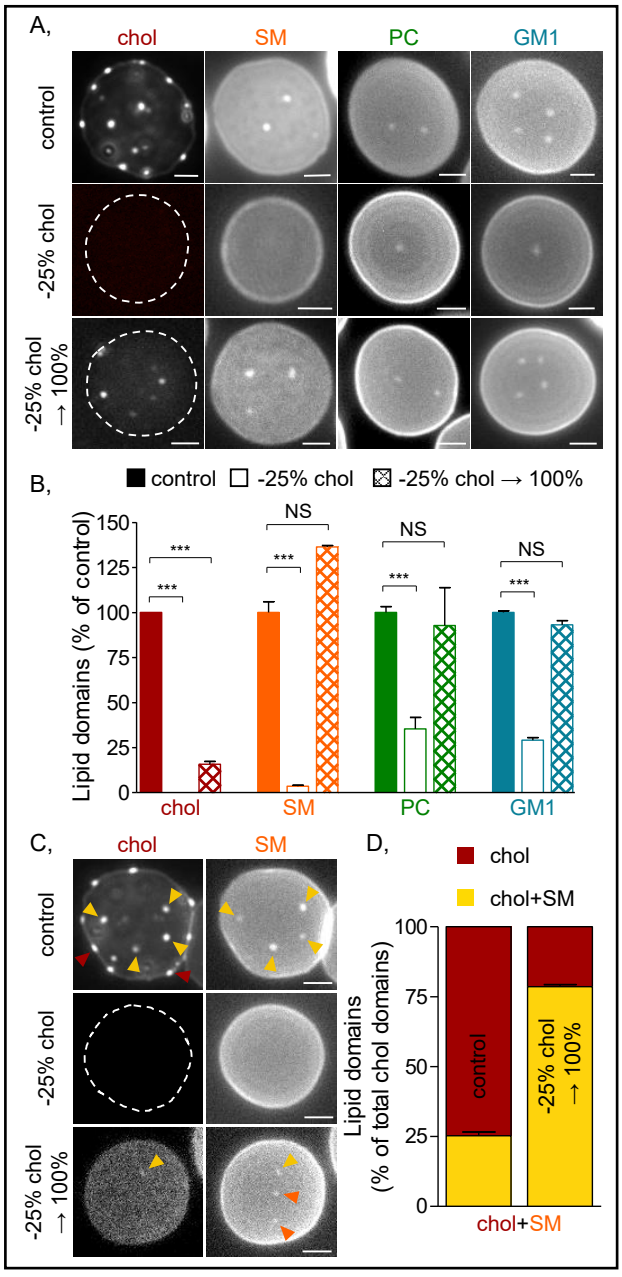

Fig. 4. All lipid domains vanish upon chol depletion and only those in low curvature areas can be restored after chol repletion. RBCs were either kept untreated (control) or chol-depleted by mβCD (0.9 mM; -25 % chol), followed or not by chol repletion (-25 % chol → 100 %) with encapsulated chol. RBCs were then either mono-labeled for chol, SM, PC or GM1 as in Fig. 1. (A, B) or double-labeled for chol and SM (C, D), spread on PLL and observed in fluorescence microscopy, all at 20°C. (A) Representative single-labeling images of different RBCs from 3 independent experiments. (B) Quantification of lipid domains in control (full bars), chol depletion (empty bars) and repletion (squared bars) conditions, expressed as percentage of the control values. Means ± SEM of 3 independent experiments where >300 RBCs were analyzed. (C) Representative double-labeling images of 2 independent experiments. Yellow arrows point to lipid domains co-enriched in chol and SM, while red and orange arrows show domains mainly enriched in chol or SM, respectively. (D) Quantification of chol- and SM-co-enriched domains (yellow portions of the bars), expressed as a percentage of the total chol-enriched domains. Means ± SEM of 2 independent experiments where >200 RBCs were analyzed. All scale bars 2 µm.

orange, green or blue columns, respectively, Fig. 3B). These results suggest that while chol-enriched domains in HC were not co-enriched in polar lipids, the majority of those located in LC was enriched in polar lipids.

To further evaluate the importance of chol for the formation and/or the maintenance of LC-associated lipid domains, we partially depleted membrane chol with methyl-β-cyclodextrin (mβCD), a cage-compound whose use on RBC membrane has been previously validated (-25 % of total membrane chol after a 0.9 mM treatment; open columns, Fig. 4B) [25]. As expected, chol-enriched domains completely disappeared under this treatment and theta* labeling was no more visible (red, Fig. 4A and B). Polar lipid domains were also affected, but to a differential extent: SM-enriched domains were almost completely abrogated while PC- and GM1-enriched domains decreased by ~65 % (orange, green and blue open columns, respectively, Fig. 4B). Hence, upon restoration of the chol content thanks to mβCD cages saturated with chol (squared columns, Fig. 4B), all polar lipid domains could be recovered.

Chol content is thus not only essential for maintenance, but also for the formation of LC-associated domains. In contrast, only a small percentage of chol-enriched domains (~15 %, red squared column, Fig. 4B) could reform upon chol repletion. As those domains were mainly located at the center of spread RBC membrane (*i.e.* in LC areas) and highly colocalized with SM-enriched domains (>75 % *vs* ~25 % in control conditions, yellow arrowheads in Fig. 4C and yellow portions of the columns in Fig. 4D), we suggest that chol-enriched domains associated with HC areas are biophysically less stable and thus require longer time or specific conditions to reform after this treatment.

We thus conclude that lipid domains associated with both HC and LC areas of the RBC outer leaflet are enriched in chol and depend on this lipid content.

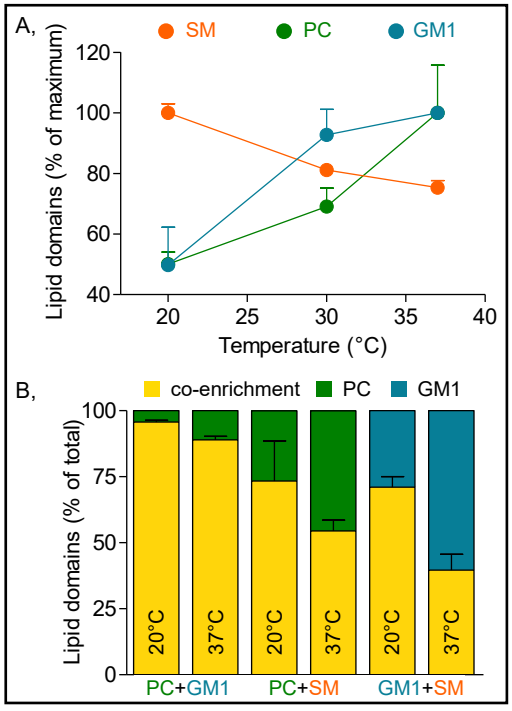

Fig. 5. In contrast to SM-enriched domains, PC- and GM1-enriched domains prevail in resting RBCs at physiological temperature. (A) Abundance of polar lipid-enriched domains at various temperatures, expressed as percentage of maximal abundance. RBCs were mono-labeled, spread and observed at the indicated temperatures. Means ± SEM of 2 independent experiments where >400 RBCs were analyzed. (B) Extent of polar lipid co-enrichment at 20°C and 37°C. Percentage of domains co-enriched in PC and GM1, PC and SM or GM1 and SM are shown as yellow portions of total PC (green)- or GM1 (blue)-enriched domains. Means ± SEM of 2 independent experiments where >200 RBCs were analyzed.

GM1/PC-enriched domains are prevalent in resting RBCs at physiological temperature

To further investigate whether lipid domains associated with LC were co-enriched or not in all polar lipids, *i.e.* SM, PC and GM1, we analyzed polar lipid domain behavior upon temperature increase between 20 and 37°C. Indeed, temperature modulates membrane fluidity and thus phase separation and lipid domain organization [36]. Two opposite behaviors could be evidenced: (i) SM-enriched domains whose number decreased by ~30 % when temperature raised from 20°C to 37°C (orange circles, Fig. 5A) in agreement with [25], *vs* (ii) PC- and GM1-enriched domains whose number doubled in the same range of temperatures (green and blue circles, Fig. 5A). By performing double labeling of polar lipids at 20°C and 37°C (Fig. 5B), we evidenced a nearly perfect colocalisation between PC- and GM1-enriched domains whatever the temperature (columns 1 and 2, Fig. 5B), while the percentages of PC- or GM1-enriched domains also enriched in SM decreased between 20°C and 37°C (columns 3 and 5 *vs* 4 and 6, Fig. 5B). Those results suggest that domains co-enriched in PC and GM1 are dominant at physiological temperature while a drop in temperature induces their co-enrichment in SM. This observation also suggests that SM-, PC- and GM1-enriched domains can be either associated or dissociated based on RBC physiological needs.

GM1-enriched domains increase in abundance upon RBC mechanical stimulation while SM-enriched domains increase thereafter upon RBC shape restoration

To further test this hypothesis, we analyzed domain abundance upon different approaches of mechanical stimulations: differential RBC spreading on PLL (Fig. 6A), hypo-osmotic swelling (Suppl. Fig. 2) and RBC (de)stretching on silicon (polydimethylsiloxane, PDMS) chambers (Fig. 6B).

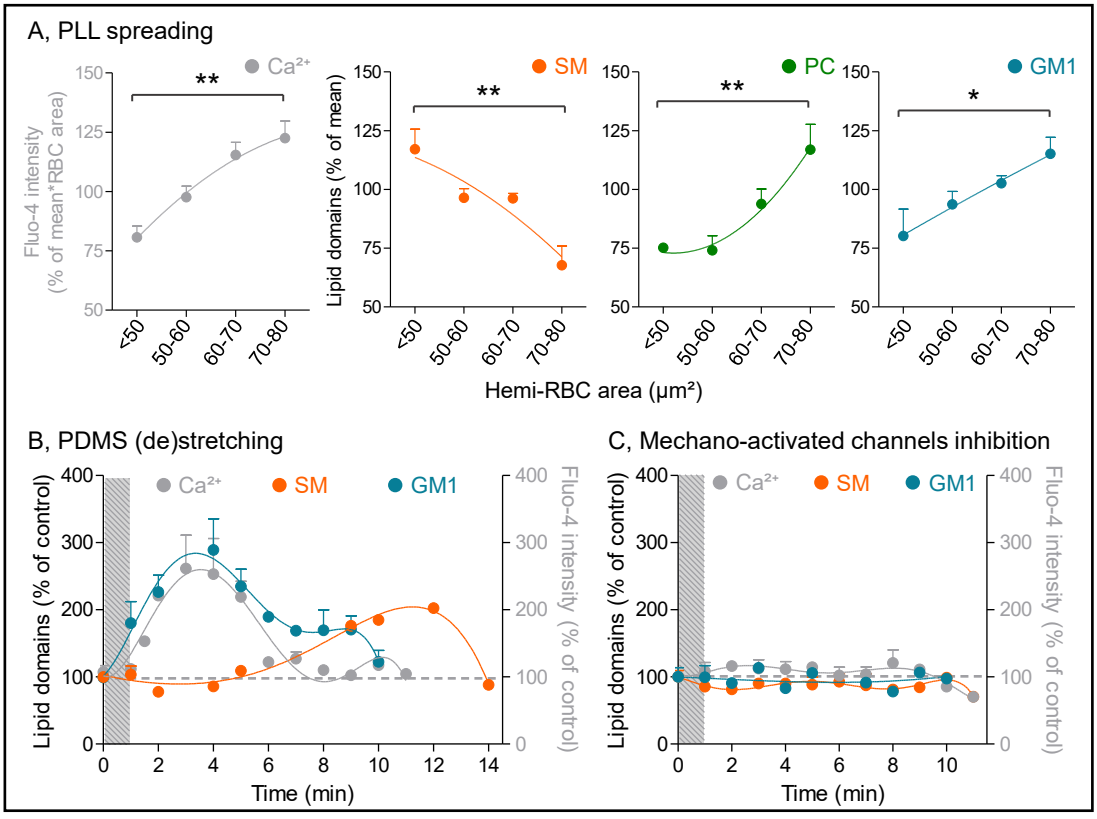

Fig. 6. PC- and GM1-enriched domains increase in abundance upon mechanical stimulation. (A) Differential spreading of RBCs on PLL. Morphometry of cell calcium content (grey dots) and domain abundance (SM, orange; PC, green; GM1, blue) under increasing projected areas of spread RBCs. RBCs were labeled at 37°C, immobilized on PLL for 4 min, washed and then let to spread for another 4 min, resulting in differential spreading (represented by different projected hemi-RBC areas). Means ± SEM of 3 independent experiments where >500 RBCs were counted. (B) (De)stretching of RBCs on silicon (PDMS) chambers. RBCs were labeled at 37°C for SM (orange dots), GM1 (blue dots) or calcium (grey dots). Lipid domains were counted and Fluo-4 intensity was measured before (t = 0 min) and after RBCs were stretched for 1 min (grey stripped zone) in PDMS chambers. Means ± SEM of 3 independent experiments where >200 RBCs were analyzed at each time. (C) (De)stretching of RBCs on PDMS chambers under inhibition of mechano-activated channels. RBCs were labeled as in (B), treated with 7 µM GsMTx4 for 15 min, stretched for 1 min (grey stripped zone) in PDMS chambers and analyzed during the indicated times upon destretching. Means ± SEM of 3 independent experiments where >100 RBCs were analyzed at each time.

We first took advantage of the differential spreading of RBCs on PLL that results from variations in the local PLL concentration, the RBC density and the adhesion duration. This heterogeneity, which was reflected in a 50 to 80 µm^2 range of immobilized RBC projected area (Fig. 6A) and a spreading-dependent accumulation of intracellular calcium (grey dots, Fig. 6A), differentially impacted lipid domains. Indeed, while PC- and GM1-enriched domains increased in abundance under RBC area increase (green and blue dots, Fig. 6A), SM-enriched domains tended to disappear (orange dots, Fig. 6A). In contrast, the abundance of chol-enriched was only slightly modified (red dots, Suppl. Fig. 3A). These observations point to the specific potential involvement of PC- and GM1-, but not SM-, enriched domains in RBC deformation upon mechanical stimulation.

We then checked whether basic mechanical stimulation by osmotic swelling could also lead to a differential modulation of lipid domains. Real-time imaging revealed the *de novo* formation of SM- and PC-enriched domains (orange and green arrowheads, Suppl. Fig. 2) shortly after the application of a hypo-osmolar medium, whereas GM1-enriched domains

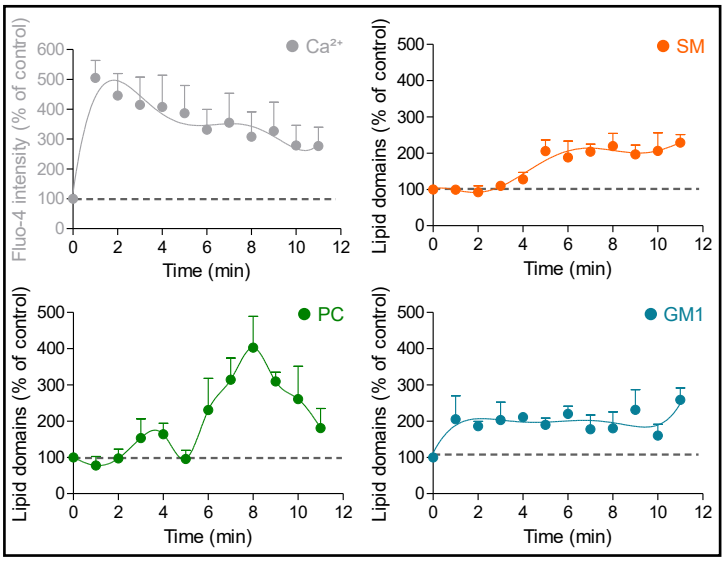

Fig. 7. PC- and GM1-enriched domains rapidly increase in abundance upon Piezo1 chemical activation while the increase in SM-enriched domains is delayed. RBCs were labeled for calcium (grey dots) or polar lipids (orange, green or blue dots) at 37°C, immobilized on PLL, treated with 0.5 µM Yoda1 for 20 sec to activate Piezo1 and immediately observed during the indicated times. Means ± SEM of 3 independent experiments for each panel where >300 RBCs were analyzed at each time.

disappeared (blue arrowhead, Suppl. Fig. 2) and chol-enriched domains remained unaffected.

Finally, we simulated RBC deformation using stretchable PDMS chambers that previously allowed us to evidence the gathering of chol-enriched domains in high-curvature membranes (Suppl. Fig. 3 B,C) and the increase of SM-enriched domains during shape restoration after deformation [29]. Immobilized RBCs were stretched for one min (grey stripped bar, Fig. 6B) and then let to recover for an additional 14 min time interval. As expected [1, 2, 29], RBC mechanical stress application occurred concomitantly with a transient intracellular calcium increase, which reached a maximal accumulation 3 min after stretching (grey dots, Fig. 6B). GM1-enriched domains showed a similar (~3fold) and transient increase (blue dots, Fig. 6B), thus perfectly coinciding with the transient calcium entry. After that, intracellular calcium decreased back to its initial concentration 6 min after stretching. From that time, the SM-enriched domain abundance started to increase (orange dots, Fig. 6B) [29].

Altogether, these results suggest that GM1-enriched domains could be linked to calcium influx during deformation whereas SM-enriched domains are linked to calcium efflux and shape restoration. This represents an additional line of evidence for the segregation between GM1- and SM-enriched domains at the RBC PM upon physiological conditions.

To further test the potential link between lipid domains and calcium exchange kinetics upon RBC deformation, we used the peptide GsMTx4, a validated inhibitor of the mechano-activated ion channels [37] which are mostly responsible for the calcium entry upon RBC deformation [1]. We showed that this treatment abolished calcium entry as well as GM1- and SM-enriched domain increase without inducing detectable toxicity (Suppl. Fig. 4). These results support our hypothesis of the correlation between GM1-enriched domain abundance and the calcium influx. Moreover, they suggest that the delayed SM-enriched domain increase is dependent on a primary calcium entry.

GM1-enriched domains are linked to Piezo1-mediated calcium influx

As GM1-enriched domains seemed to be involved into the deformation-dependent calcium influx, we explored the potential link between those domains and Piezo1. This non-selective mechano-activated cation channel plays a key role in the RBC deformation-dependent calcium influx and the following cellular volume regulation [3]. To test this hypothesis, RBCs were treated for 20 sec with Yoda1, a small agonist of this channel [38]. As expected, an immediate strong increase of the intracellular calcium concentration was observed (grey dots, Fig. 7) without detectable signs of toxicity (Suppl. Fig. 4). Intracellular calcium concentration then slowly decreased, suggesting the activation of the calcium efflux mechanisms and/or a possible slow desorption of Yoda1. The immediate increase

of intracellular calcium was concomitant with a 2-fold increase of GM1-enriched domains (blue dots, Fig. 7), while the SM-enriched domain increase was delayed and only appeared 5 min after the treatment (orange dots, Fig. 7). PC-enriched domains showed an intermediate behavior, with a first slight increase 3 min after the treatment followed by a second, more important, increase after 6 min (green dots, Fig. 7).

From all these data, we concluded that GM1-enriched domains, but not those enriched in SM, are closely linked to the Piezo1-mediated calcium entry into RBC upon deformation.

SM/PC-enriched domain abundance is closely related to the secondary calcium efflux and/or the extent of the membrane:cytoskeleton anchorage

The delayed increase of SM-enriched domains and the intermediate behavior of PC-enriched domains under Yoda1 activation suggested that not only SM- but also PC-enriched domains might contribute to secondary calcium efflux. In RBCs, this efflux is exclusively operated by the energy-dependent PMCA. This pump is regulated by calmodulin binding (and thus intracellular calcium concentration) but also by calpain cleavage, intracellular domain modifications and even acidic lipids from the inner leaflet [39].

To test an eventual link between SM- and PC-enriched domains and PMCA activation, secondary calcium efflux was stimulated without activating the Piezo1-mediated influx. In 2002, Andrews and collaborators reported that the treatment of RBCs with a phorbol ester stimulates a protein kinase C (PKC) mediated $Ca_v2.1$-like calcium permeability pathway [40]. As this calcium entry is Piezo1-independent, we speculated that SM- and PC-, but not GM1-enriched domains, would be increased by this treatment. We thus used phorbol myristate acetate (PMA, a diacylglycerol analog) and calyculin A (CalA, a phosphatase inhibitor) to activate PKC. As expected, we observed a slight increase of intracellular calcium (data not shown) as well as a ~2-fold increase of SM- and PC-enriched domains that contrasted with the decrease of GM1-enriched domains (images in Fig. 8A and quantification in Fig. 8B).

We then stimulated calcium efflux in a more direct approach. To this aim, we used the calcium chelator EGTA to remove all traces of calcium in the extracellular medium (Fig. 8A, C) [29]. This treatment induced an important decrease of intracellular calcium (-95 % of control fluorescence, data not shown) and led to a ~2.5 fold increase of SM-enriched domains, as previously reported [29], but also a ~1.8 fold increase of PC-enriched domains (empty bars, Fig. 8C). The GM1-enriched domains were, on the other hand, decreased by this treatment, supporting the hypothesis of their involvement in calcium influx but not in its efflux. This treatment seemed not toxic since RBC re-incubation in 1.8 mM calcium-containing medium fully restored domain abundance (squared bars, Fig. 8C) and since hemoglobin release remained unchanged as compared to untreated RBCs (Suppl. Fig. 4).

We next aimed to target the PMCA pump by depleting the RBC energy content by incubation in a glucose-free medium for 2 h (Fig. 8D). This treatment, which led to a 75% decrease of the RBC ATP content (from ~2-3 mM in control cells to ~500-750 µM in depleted cells, data not shown), was not sufficient to directly inhibit the PMCA (K_M for ATP, ~3 µM). Nevertheless and in agreement with [41] and [42], it was able to indirectly impair the PMCA. Indeed, while calcium initial content was fully restored 6 min after stretching in control RBCs (see Fig. 6B and full grey points in Fig. 8E), it could not be restored even after 12 min in energy-deprived RBCs (empty grey points in Fig. 8E). Surprisingly, this PMCA inhibition also induced a high increase of SM- and PC-enriched domains, while GM1-enriched domains were not affected (empty bars, Fig. 8D). We can reasonably exclude toxicity to explain this observation, as revealed by the reversibility of the ATP depletion effect (squared bars, Fig. 8D) and the low hemoglobin release (Suppl. Fig. 4). Those results could be related to the increase of reactive oxygen species (ROS) upon energy privation through the inhibition of the anti-oxidant enzymes like the glutathione synthase (K_M for ATP, ~400 µM, [43]). Produced ROS might in turn disturb the PMCA, but also the membrane:cytoskeleton anchorage. This hypothesis is discussed in the last section of the Discussion but remains to be tested.

Our results suggest that while SM- and PC-enriched domains increase in abundance upon calcium efflux and/or cytoskeleton modulation, those enriched in GM1 are instead

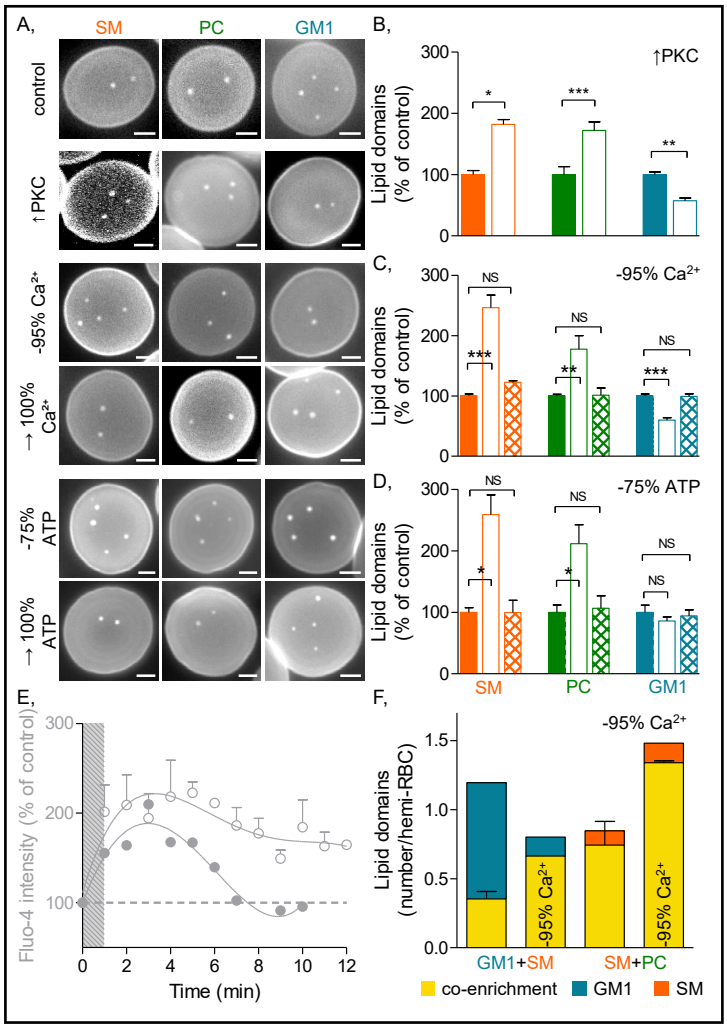

Fig. 8. Unlike GM1-enriched domains, SM- and PC-enriched domains increase upon secondary calcium efflux and/or membrane:cytoskeleton impairment. RBCs were either (i) kept untreated (control); (ii) treated with a phorbol ester (PMA, 6 µM) and a phosphatase inhibitor (CalA, 20 nM; ↑ PKC); (iii) incubated in a calcium-free medium containing 1 mM EGTA (-95 % Ca^{2+}), followed or not by reincubation in calcium-containing medium (→ 100 % Ca^{2+}); or (iv) incubated in a glucose-free medium for 2 h (-75 % ATP), followed or not by reincubation in a glucose-containing medium (→ 100 % ATP). All RBCs were then spread and labeled for polar lipids at 37°C. (A) Representative images. Scale bars 2 µm. (B-D) Quantification of lipid domains in control RBCs (plain bars), under treatment (empty bars) and in repletion conditions (squared bars). Means ± SEM of 3 independent experiments where >300 RBCs were analyzed. (E) Control (plain dots) and ATP-depleted (empty dots) RBCs were labeled for calcium at 37°C, stretched for 1 min (grey stripped zone) in PDMS chambers and analyzed during the indicated times upon destretching. (F) Double labeling between GM1 and SM or SM and PC on RBCs upon intracellular calcium depletion at 37°C. Percentage of domains double-enriched in GM1 and SM or in SM and PC are shown as yellow portions of total GM1 (blue)- or SM (orange)-enriched domains.

unaffected or even decreased. Hence, they suggest the association between SM- and PC-enriched domains upon calcium efflux, at the detriment of GM1-enriched domains. This was confirmed by double-labeling of RBCs upon EGTA treatment. Indeed, GM1-enriched domains that were not co-enriched in SM decreased (blue columns, Fig. 8F) as new lipid domains co-enriched in SM and PC, but not in GM1, were formed (orange columns, Fig. 8F).

Polar lipid domain integrity is needed for calcium exchanges at the RBC surface

Finally, we questioned whether polar lipid-enriched domains were only modulated through, or needed for, calcium exchanges at the RBC PM by abrogating lipid domains. We first used mβCD, which disrupted all lipid domains at moderate concentration (0.9- 1 mM, -25 % chol, see Fig. 4B). Under this concentration, calcium entry upon RBC stretching in silicon chambers was completely inhibited (from a 2.7-fold increase of fluorescence in untreated RBCs to no increase in mβCD-treated RBCs, grey dot at 1 mM, Fig. 9A). At a lower mβCD concentration (0.5 mM, -15 % chol, empty dot, Fig. 9A), chol- and SM-enriched domains were already disrupted (red and orange dots at 0.5 mM, Fig. 9A), while PC and GM1-enriched domains were not affected (green and blue dots at 0.5 mM). At this concentration, calcium

entry was non-significantly decreased (from a 2.7-fold increase of fluorescence in untreated RBCs to a 2.4-fold increase upon mβCD treatment, grey dot at 0.5 mM, Fig. 9A), indicating that RBCs were still able to respond to stretching by a calcium entry. The abolition of the stretching-induced calcium increase at 1 mM could result from the absence of resting-state GM1/PC-enriched domains for the primary Piezo1 activation or from the impossibility for these domains to get formed around Piezo1 under activation to sustain an efficient calcium entry. However, we cannot discard the possibility that this effect only resulted from the slight (~8 %) decrease of the chol content between 0.5 mM and 1 mM mβCD.

Finally, we used sphingomyelinase (SMase), a hydrolase catalyzing the breakdown of SM and allowing to decrease the PM SM content by up to 60 % (empty dots, Fig. 9B) without detectable cell toxicity [26]. We showed that a moderate SM depletion (-30 % at 3 mU/ml) led to the nearly complete disappearance of SM-enriched domains (-90 %, orange dots, Fig. 9B) and a ~2-fold increase of intracellular calcium (grey dots, Fig. 9B). As a matter of fact, the decrease of SM domains upon SMase treatment was proportional (R^2=0.9553) to the intracellular calcium increase. These data suggest that SM-enriched domains are not only a marker of active calcium extrusion, but are also required to maintain a low intracellular calcium concentration.

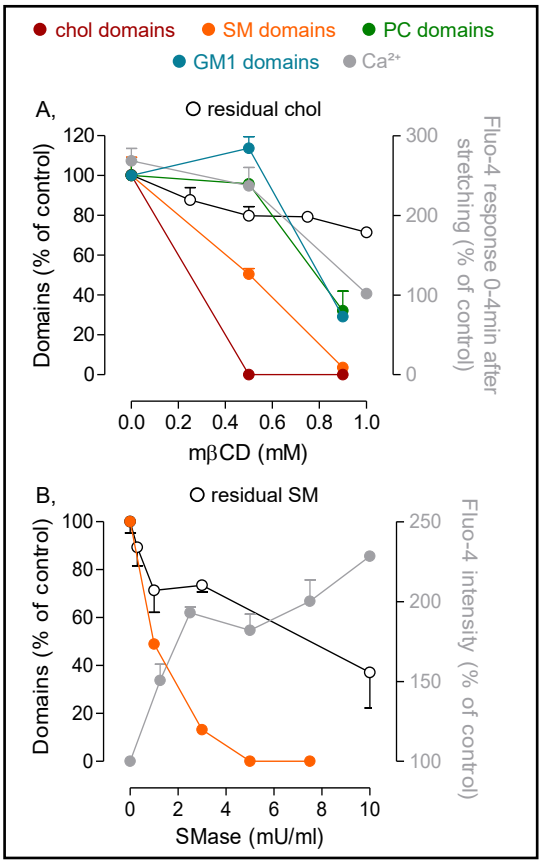

Fig. 9. Intracellular calcium content is altered upon lipid domain abrogation. (A) RBCs were treated in suspension with the indicated concentrations of mβCD and either (i) directly analyzed for chol residual content (empty dots); or (ii) spread onto PLL-coverslips for analysis of lipid domain abundance (red, orange, green or blue dots) at 37°C; or (iii) laid down on PDMS chambers and analyzed 2 min after stretching for intracellular calcium (expressed as the percentage of calcium content in unstretched RBCs; grey symbols). (B) RBCs were treated in suspension with the indicated concentrations of sphingomyelinase (SMase) and (i) directly analyzed for SM residual content (open dots) and intracellular calcium content (grey dots) at 37°C; or (ii) spread onto PLL-coated coverslips for SM-enriched domain abundance at 37°C counting (orange dots). Means ± SEM of 2-3 independent experiments where >200 RBCs were analyzed.

Discussion

In the last decades, evidence for lipid domains of various composition at the surface of several cells has emerged. First transient nanometric domains enriched in sphingolipids and chol [11] and then more stable and larger domains that could exhibit a differential lipid composition than rafts. In the last few years, we evidenced and characterized two types of submicrometric lipid domains at the RBC surface, mainly enriched in chol and/or SM [25, 26, 29]. We here extended this study to PC and GM1, two other main lipids of the outer PM leaflet, and mapped their relationship and functional relevance.

Lipid domain diversity at resting state

Based on previous results on chol- and SM-enriched domains and on the new data we acquired on PC- and GM1-enriched domains, we suggest the coexistence of three populations of lipid domains in RBCs at resting state at physiological temperature: (i) mostly chol-enriched ones, abundant (~8/hemi-RBC), HC-associated and exhibiting high lipid order; (ii) GM1/PC/chol-enriched ones, less abundant (~1.5/hemi-RBC), LC-located and presenting lower ordering; and (iii) SM/PC/chol-enriched ones, rare (~0.6/hemi-RBC), also LC-located and with low ordering. Considering the wide range of domain features that lipid-lipid interactions can generate in molecular simulations of simple and complex bilayers, it is not so surprising to unveil such a diversity of lipid domains in living cell membranes. As a matter of fact, lipid clusters in simulated membranes show various (i) composition, as they are not only enriched in SM and chol, but also in gangliosides (GM1 and GM3) and in PC analogs [44, 45]; (ii) lipid order; and (iii) topography, as some GM3 nano-clusters have been shown to preferentially associate with concave (when viewed from the extracellular medium) membranes [46]. Such lipid domain diversity is also supported by several experimental data on simple lipid mixtures [47-49].

Direct lipid:lipid interactions could be able to induce lipid clusters in systems devoid of proteins and certainly help to understand some of the lipid domain behaviors that we evidenced on RBCs. For example, differential temperature dependence between GM1- and PC-enriched domains *vs* those enriched in SM is partly explainable by individual lipid intrinsic properties (*e.g.* head group, acyl chain length and saturation [50]). Moreover, lipid domain biogenesis and/or maintenance also depend on the chol content, as chol is a key regulator of membrane fluidity (and thus space between phospholipids for optimal head group interactions) and is able to directly interact with SM or GM1 [45, 51].

In a complex active system including lipids and proteins like living cell membranes, it is however unlikely that such lipid:lipid interactions are the only key regulators of lipid domains. We previously proposed several regulators for chol-enriched domains located in RBC HC areas [29]. We will here focus on the LC-associated lipid domains. The maintenance of GM1/PC/chol- and SM/PC/chol-enriched domains at a low level in LC areas of RBCs at resting state could involve membrane:cytoskeleton anchorage and/or charge-mediated interactions. Lipid domain stability in time and space at resting state supports the hypothesis of their restriction by anchorage of the membrane to the spectrin cytoskeleton, either via direct interactions with anchorage complex proteins or via an inner PM leaflet coupling. The strong dependence of SM/PC/chol-enriched domains to the intracellular calcium increase (either after stretching in PDMS chambers or under pharmacological treatments) suggests their restriction through the 4.1R anchorage complex. Indeed, anchorage through 4.1R complex is strongly decreased following calcium increase, as the binding of calmodulin/calcium to the proteins of this complex decreases their affinity for each other [2]. PKC activation and ATP depletion also led to the modulation of the anchorage through 4.1R, and SM/PC-enriched domains were also highly sensitive to those two treatments. GM1/PC/chol-enriched domains seemed on the other hand closely linked to the ankyrin-based anchorage complexes (our unpublished data).

Lipid domain modulation upon stretching and calcium exchanges

The three domain populations did not exhibit the same response to stimuli applied to the RBCs. Chol-enriched domains gather in increased curvature areas upon RBC deformation but do not increase in abundance. They could be involved in creating/maintaining HC areas needed for RBC deformation (red domains, Fig. 10) [29]. In contrast, both GM1/PC/chol- and SM/PC/chol-enriched domains were strongly increased during calcium exchanges accompanying RBC (re)shaping process, but in different kinetics. To the best of our knowledge, this is the first time that lipid domains of the external PM leaflet are proposed to contribute to calcium exchanges, crucial for the RBC to gain in flexibility when it is subjected to mechanical stress (*e.g.* in small capillaries or in the spleen). Indeed, a transient calcium influx will lead to the Gardos channel activation and a consequent cell dehydration, increasing the surface/volume

ratio and favoring cell deformation (Fig. 10) [1]. The importance of calcium for RBC mechanical stability and deformation is further illustrated by the demonstration that permanent calcium upregulation, linked to uncontrolled impairment of cytoskeletal density and/or anchorage (*e.g.* in RBCs of patients with haemolytic anemia), compromises mechanical stability of the RBC membrane [52].

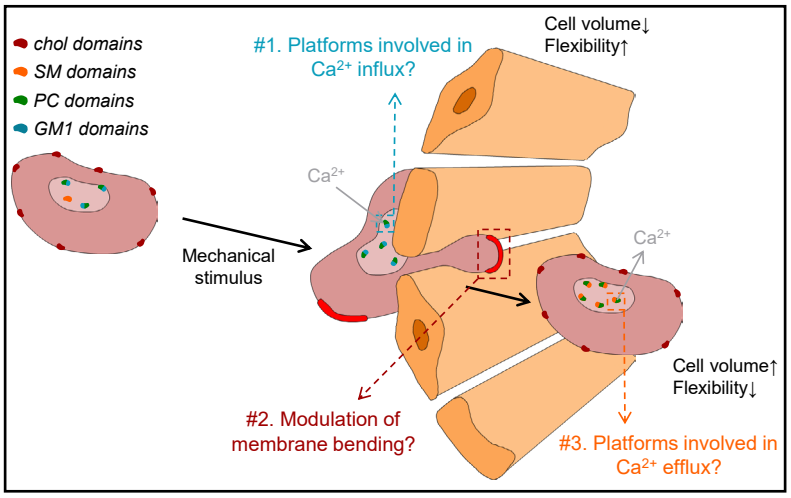

Fig. 10. Evidence-based hypothetical model of the contribution of lipid domains to RBC deformation. Under mechanical stress (e.g. in the spleen sinusoids), GM1/PC-enriched domains (blue/green) increase to favor calcium influx while chol-enriched domains (red) gather in the high-curvature membrane and modulate membrane bending. At the same time, cell volume decreases via activation of the Gardos channels and the RBC flexibility increases via uncoupling between membrane and the cytoskeleton at the 4.1R complexes. The cell volume is restored after the end of the stress application by calcium efflux thanks to the contribution of SM/PC-enriched domains (orange/green).

Calcium influx can occur through several channels like Piezo1, Cav2.1 and TRPC (*i.e.* transient receptor potential cation channel). Piezo1, a mechanically-activated cation channel, has been evidenced to play the major role in RBC deformation-induced calcium increase [3]. Moreover, mutations in Piezo1 causing an increased cation permeability have been linked to hereditary xerocytosis where RBCs are dehydrated [53]. Here, we show a close relation between the number of GM1/PC/chol-enriched domains at the RBC surface and the activation state of Piezo1 (blue/green, domains, Fig. 10), based on three lines of evidence: (i) the strong increase of lipid domain abundance under RBC stretching, which is inhibited by a mechano-activated channel inhibitor; (ii) the same increase under the chemical Piezo1 activation; and (iii) the concomitant inhibition of the stretching-mediated calcium entry and abrogation of domains under chol depletion.

SM/PC/chol-enriched domains seem also to be related to calcium exchanges, not during its influx but instead during its efflux (orange/green domains, Fig. 10). Calcium efflux is as important as influx since a prolonged calcium increase will lead to the RBC senescence and removal from the blood [2]. The involvement of SM/PC/chol-enriched domains in calcium efflux is based on the following evidences. First, they exhibit a delayed increase in abundance upon calcium entry (either by stretching or chemical activation). Second, they specifically increase in abundance when secondary calcium efflux is activated (either via PMA/CalA or EGTA treatment).

Lipid domains as modulators of Piezo1 and PMCA membrane localization and/or activity?

Sorting and activation of membrane proteins is the most studied function of lipid domains [54-57]. These effects can be attributed either to the modification of bilayer properties (thickness, curvature or surface tension) or to the binding of specific lipids to the protein surface. It is easily imaginable that mechanically-activated channels like Piezo could be affected by the surrounding membrane properties. Their activity have already been shown to be highly dependent on the membrane stiffening [58] and thus the membrane chol

content, but also on the level of fatty acid saturation [59]. Moreover, new insights in Piezo1 structure evidenced a bend in its transmembrane section [60], whose stabilization energy might be partly compensated by the surrounding lipids.

Based on the results presented in this article, we suggest that GM1/PC/chol-enriched domains could contribute to the regulation of Piezo1 by modulating its environment biophysical properties to allow an efficient and transient calcium influx. This is based on the three following facts. First, GM1 are inverted cone shaped lipids and the bend evidenced in the structure of Piezo1 at resting state supports the possibility that Piezo1 rests in a locally curved lipid bilayer environment, while upon rising membrane tension, the reduction of curvature could open the pore. Second, domains co-enriched in GM1 and chol should present a higher thickness than other domains, which could favor the recruitment/stabilization of Piezo1 transmembrane domains [61]. Indeed, a mechanically-activated protein has recently been shown to have a more expanded constriction pore in the presence of a positive mismatch (thicker lipids) than in negative mismatch (thinner lipids) [62]. Third, GM1-enriched domains appear dependent on the anchorage through ankyrin (our unpublished data) and the cytoskeleton is known to modulate Piezo1 activity [63].

While the sequence of events linking lipid domains to Piezo1 remains to be elucidated, several hypotheses can be suggested. First, GM1/PC/chol domains could be formed following the calcium ion influx and represent a secondary event. However, the fact that a Piezo1-independent calcium influx, as achieved through PKC activation [40], instead induced a decrease of GM1-enriched domains does not support this hypothesis. Second Piezo1 could modulate its surrounding environment upon activation by recruiting specific lipids such as GM1 and chol, forming domains which might modify Piezo1 dynamic properties and allow an efficient and transient calcium influx. Third, Piezo1 could be preferentially localized in GM1/PC/chol-enriched domains in RBCs at resting state, an association necessary for the primary activation of the channel. Simulation studies and localization experiments are needed to investigate these hypotheses.

While the results we present in this article suggest a correlation between calcium efflux and SM/PC/chol-enriched domain abundance, their specific role in PMCA regulation remains to be elucidated. We here propose two non-mutually exclusive hypotheses. On one hand, as for Piezo1, SM/PC/chol-enriched domains could represent a favorable environment for the protein activity. This could be linked to (i) the domain specific biophysical properties (*e.g.* lipid order); (ii) the strength of their cytoskeleton anchorage; and/or (iii) their correspondence with specific lipids in the inner leaflet, *a.o.*. The membrane lipid order hypothesis is supported by (i) our present observation that SM/PC/chol-enriched domains were more disordered than the rest of the membrane; (ii) our previous observation that lipid domain order increases to a bigger extent than the bulk membrane order upon stimulation of calcium efflux by treatment of RBCs with EGTA [31]; and (iii) several studies in model membranes, although with sometimes conflicting information. For instance, PMCA activity is decreased in highly-ordered areas of liposomes made of PC/SM/chol [64] but is favored in highly ordered lens fiber lipids in comparison with disordered DOPC liposomes [65]. Besides membrane fluidity, SM/PC/chol-enriched domains could contribute to the regulation of PMCA activity through the reversible and controlled modulation of membrane:cytoskeleton anchorage upon deformation-induced calcium entry. As a matter of fact, the protein 4.1R has been shown to directly interact with PMCA1 and to be essential for its activity in enterocytes [66]. The close relationship between the membrane:cytoskeleton anchorage, the PMCA activity and the SM/PC/chol-enriched domains could partly explain the *a priori* contradictory results we obtained by stimulating the PMCA through PKC activation *vs* impairing the pump through ATP depletion. Indeed, both treatments could induce the uncoupling of the membrane:cytoskeleton anchorage (by phosphorylation of the 4.1R complexes *vs* potential increase of ROS damages) and the increase of calcium (by stimulating a Piezo1-independent calcium influx *vs* indirectly impairing the PMCA) together with a secondary membrane:cytoskeleton uncoupling (by calmodulin binding). One hypothesis is that the reversibility of lipid domain abundance increase depends on the transient

membrane:cytoskeleton uncoupling, which became permanent under the two treatments, resulting into an incapacity to de-form the domains. Finally, SM/PC/chol-enriched domains at the external PM leaflet could contribute to the regulation of PMCA activity through their potential coupling with specific lipids in the inner PM leaflet, known to regulate PMCA activity [67, 68]. For example, electrostatic interactions and subsequent clustering of PIP_2 at the inner leaflet have been shown to be induced by a local calcium increase [69]. This could in turn induce a transbilayer clustering in superposition in the outer leaflet resulting into SM-enriched domain formation, as shown by super-resolution microscopy [70].

On the other hand, SM/PC/chol-enriched domains might modulate the PM distribution of PMCA to protect the pump from the reactions with ROS. Indeed, PMCA activity has been shown to be decreased by direct oxidation [71] or by binding of oxidized calmodulin [72]. This oxidation leads to conformational changes and the formation of aggregates that cannot recover their activity [73]. SM, on the other hand, is proposed to be a natural antioxidant that inhibits the peroxidation of unsaturated phospholipids and chol [74].

Altogether, our study opens new avenue to explore the importance of PM lipid domains in cell deformation associated to other physiological processes, such as the phagocytic cup, the immunological synapse, cell division or migration and invasion.

Abbreviations

BODIPY (*N*-(4,4-Difluoro-5,7-Dimethyl-4-Bora-3a,4a-Diaza-*s*-Indacene-3- Pentanoyl)); BSA (bovine serum albumin); CalA (calyculin A); Chol (cholesterol); FASTDil (1,1'-Dilinoleyl-3,3,3',3'-Tetramethylindocarbocyanine, 4-Chlorobenzenesulfonate); DMEM (Dulbecco's Modified Eagle Medium); EGTA (ethylene glycol-bis(β-aminoethyl ether)-N,N,N',N'-tetraacetic acid); FCS (fluorescence correlation spectroscopy); GM1 (monosialotetrahexosylganglioside); GP (generalized polarization); HC (high curvature); Laurdan (2-dimethylamino-6-lauroylnaphthalene); LC (low curvature); mβCD (methyl-β-cyclodextrin); PC (phosphatidylcholine); PDMS (polydimethylsiloxane); PKC (protein kinase C); PLL (poly-L-lysine); PM (plasma membrane); PMA (phorbol myristate acetate); PMCA (plasma membrane calcium ATPase); RBC (red blood cell); ROS (reactive oxygen species); SM (sphingomyelin); SMase (sphingomyelinase)

Acknowledgements

We thank Drs. A. Miyawaki, M. Abe and T. Kobayashi (Riken Brain Science Institute, Saitama, Japan & University of Strasbourg, France) as well as H. Mizuno (KU Leuven, Belgium) for generously supplying the Dronpa-NT-Lysenin and Dronpa-theta-D4 plasmids. We thank Pr. P. Gailly (Institute of Neuroscience, Université catholique de Louvain, Belgium) for providing us a mechanical cell strain instrument for PDMS chambers. J. Steinkühler was supported by the MaxSynBio consortium, which is jointly funded by the Federal Ministry of Education and Research (BMBF) of Germany (FKZ 031A359L) and the Max Planck Society (MPG). This work was supported by belgian grants from UCLouvain (FSR and Actions de Recherches concertées, ARC), F.R.S-FNRS and Salus Sanguinis foundation.

Disclosure Statement

The authors declare they have no conflict of interest.

References

1 Danielczok JG, Terriac E, Hertz L, Petkova-Kirova P, Lautenschlager F, Laschke MW, Kaestner L: Red Blood Cell Passage of Small Capillaries Is Associated with Transient Ca(2+)-mediated Adaptations. Front Physiol 2017;8:979-990.
2 Bogdanova A, Makhro A, Wang J, Lipp P, Kaestner L: Calcium in red blood cells-a perilous balance. Int J Mol Sci 2013;14:9848-9872.
3 Cahalan SM, Lukacs V, Ranade SS, Chien S, Bandell M, Patapoutian A: Piezo1 links mechanical forces to red blood cell volume. Elife 2015;4:e07370.
4 Klinken P: Red blood cells. Int J Biochem Cell Biol 2002;34:1513-1518.
5 Mohandas N, Gallagher PG: Red cell membrane: past, present, and future. Blood 2008;112:3939-3948.
6 Viallat A, Abkarian M: Red blood cell: from its mechanics to its motion in shear flow. Int J Lab Hematol 2014;36:237-243.
7 Byers TJ, Branton D: Visualization of the protein associations in the erythrocyte membrane skeleton. Proc Natl Acad Sci U S A 1985;82:6153-6157.
8 Uyuklu M, Meiselman HJ, Baskurt OK: Effect of decreased plasma cholesterol by atorvastatin treatment on erythrocyte mechanical properties. Clin Hemorheol Microcirc 2007;36:25-33.
9 Carquin M, D'Auria L, Pollet H, Bongarzone ER, Tyteca D: Recent progress on lipid lateral heterogeneity in plasma membranes: From rafts to submicrometric domains. Prog Lipid Res 2016;62:1-24.
10 Simons K, Vaz WL: Model systems, lipid rafts, and cell membranes. Annu Rev Biophys Biomol Struct 2004;33:269-295.
11 Lingwood D, Simons K: Lipid rafts as a membrane-organizing principle. Science 2010;327:46-50.
12 Janes PW, Ley SC, Magee AI, Kabouridis PS: The role of lipid rafts in T cell antigen receptor (TCR) signalling. Semin Immunol 2000;12:23-34.
13 Sydor AM, Czymmek KJ, Puchner EM, Mennella V: Super-Resolution Microscopy: From Single Molecules to Supramolecular Assemblies. Trends Cell Biol 2015;25:730-748.
14 Godin AG, Lounis B, Cognet L: Super-resolution microscopy approaches for live cell imaging. Biophys J 2014;107:1777-1784.
15 Hell SW, Sahl SJ, Bates M, Zhuang X, Heintzmann R, Booth MJ, Bewersdorf J, Shtengel G, Hess H, Tinnefeld P: The 2015 super-resolution microscopy roadmap. J Phys D Appl Phys 2015;48:443001-443002.
16 de Almeida RF, Loura LM, Prieto M: Membrane lipid domains and rafts: current applications of fluorescence lifetime spectroscopy and imaging. Chem Phys Lipids 2009;157:61-77.
17 Abe M, Kobayashi T: Imaging local sphingomyelin-rich domains in the plasma membrane using specific probes and advanced microscopy. Biochim Biophys Acta 2013;1841:720-726.
18 Mizuno H, Abe M, Dedecker P, Makino A, Rocha S, Ohno-Iwashita Y, Hofkens J, Kobayashi T, Miyawaki A: Fluorescent probes for superresolution imaging of lipid domains on the plasma membrane. Chem Sci 2011;2:1548-1553.
19 Barak I, Muchova K: The role of lipid domains in bacterial cell processes. Int J Mol Sci 2013;14:4050-4065.
20 Toulmay A, Prinz WA: Direct imaging reveals stable, micrometer-scale lipid domains that segregate proteins in live cells. J Cell Biol 2013;202:35-44.
21 Malinsky J, Opekarova M, Tanner W: The lateral compartmentation of the yeast plasma membrane. Yeast 2010;27:473-478.
22 Mound A, Lozanova V, Warnon C, Hermant M, Robic J, Guere C, Vie K, Lambert de Rouvroit C, Tyteca D, Debacq-Chainiaux F, Poumay Y: Non-senescent keratinocytes organize in plasma membrane submicrometric lipid domains enriched in sphingomyelin and involved in re-epithelialization. Biochim Biophys Acta 2017;1862:958-971.
23 Frisz JF, Lou K, Klitzing HA, Hanafin WP, Lizunov V, Wilson RL, Carpenter KJ, Kim R, Hutcheon ID, Zimmerberg J, Weber PK, Kraft ML: Direct chemical evidence for sphingolipid domains in the plasma membranes of fibroblasts. Proc Natl Acad Sci U S A 2013;110:613-622.
24 Tyteca D, D'Auria L, Van Der Smissen P, Medts T, Carpentier S, Monbaliu JC, de Diesbach P, Courtoy PJ: Three unrelated sphingomyelin analogs spontaneously cluster into plasma membrane micrometric domains. Biochim Biophys Acta 2010;1798:909-927.
25 Carquin M, Conrard L, Pollet H, Van Der Smissen P, Cominelli A, Veiga-da-Cunha M, Courtoy PJ, Tyteca D: Cholesterol segregates into submicrometric domains at the living erythrocyte membrane: evidence and regulation. Cell Mol Life Sci 2015;72:4633-4651.

26 Carquin M, Pollet H, Veiga-da-Cunha M, Cominelli A, Van Der Smissen P, N'Kuli F, Emonard H, Henriet P, Mizuno H, Courtoy PJ, Tyteca D: Endogenous sphingomyelin segregates into submicrometric domains in the living erythrocyte membrane. J Lipid Res 2014;55:1331-1342.
27 D'Auria L, Van Der Smissen P, Bruyneel F, Courtoy PJ, Tyteca D: Segregation of fluorescent membrane lipids into distinct micrometric domains: evidence for phase compartmentation of natural lipids? PLoS One 2011;6:e17021.
28 Dumitru A, Poncin M, Conrard L, Dufrêne Y, Tyteca D, Alsteens D: Nanoscale membrane architecture of healthy and pathological red blood cells. Nanoscale Horizons 2018;3:293-304.
29 Leonard C, Conrard L, Guthmann M, Pollet H, Carquin M, Vermylen C, Gailly P, Van Der Smissen P, Mingeot-Leclercq MP, Tyteca D: Contribution of plasma membrane lipid domains to red blood cell (re)shaping. Sci Rep 2017;7:4264-4281.
30 Owen DM, Rentero C, Magenau A, Abu-Siniyeh A, Gaus K: Quantitative imaging of membrane lipid order in cells and organisms. Nat Protoc 2011;7:24-35.
31 Leonard C, Pollet H, Vermylen C, Gov N, Tyteca D, Mingeot-Leclercq MP: Tuning of Differential Lipid Order Between Submicrometric Domains and Surrounding Membrane Upon Erythrocyte Reshaping. Cell Physiol Biochem 2018;48:2563-2582.
32 Kaestner L, Tabellion W, Weiss E, Bernhardt I, Lipp P: Calcium imaging of individual erythrocytes: problems and approaches. Cell Calcium 2006;39:13-19.
33 D'Auria L, Fenaux M, Aleksandrowicz P, Van Der Smissen P, Chantrain C, Vermylen C, Vikkula M, Courtoy PJ, Tyteca D: Micrometric segregation of fluorescent membrane lipids: relevance for endogenous lipids and biogenesis in erythrocytes. J Lipid Res 2013;54:1066-1076.
34 Parasassi T, Gratton E: Membrane lipid domains and dynamics as detected by Laurdan fluorescence. J Fluoresc 1995;5:59-69.
35 Sanchez SA, Tricerri MA, Gratton E: Laurdan generalized polarization fluctuations measures membrane packing micro-heterogeneity *in vivo*. Proc Natl Acad Sci U S A 2012;109:7314-7319.
36 van Meer G, Voelker DR, Feigenson GW: Membrane lipids: where they are and how they behave. Nat Rev Mol Cell Biol 2008;9:112-124.
37 Gnanasambandam R, Ghatak C, Yasmann A, Nishizawa K, Sachs F, Ladokhin AS, Sukharev SI, Suchyna TM: GsMTx4: Mechanism of Inhibiting Mechanosensitive Ion Channels. Biophys J 2017;112:31-45.
38 Syeda R, Xu J, Dubin AE, Coste B, Mathur J, Huynh T, Matzen J, Lao J, Tully DC, Engels IH, Petrassi HM, Schumacher AM, Montal M, Bandell M, Patapoutian A: Chemical activation of the mechanotransduction channel Piezo1. Elife 2015;4:e07369.
39 Lopreiato R, Giacomello M, Carafoli E: The plasma membrane calcium pump: new ways to look at an old enzyme. J Biol Chem 2014;289:10261-10268.
40 Andrews DA, Yang L, Low PS: Phorbol ester stimulates a protein kinase C-mediated agatoxin-TK-sensitive calcium permeability pathway in human red blood cells. Blood 2002;100:3392-3399.
41 Bruce J: Plasma membrane calcium pump regulation by metabolic stress. World J Biol Chem 2010;1:221-228.
42 Barrow SL, Voronina SG, da Silva Xavier G, Chvanov MA, Longbottom RE, Gerasimenko OV, Petersen OH, Rutter GA, Tepikin AV: ATP depletion inhibits Ca2+ release, influx and extrusion in pancreatic acinar cells but not pathological Ca2+ responses induced by bile. Pflugers Arch 2008;455:1025-1039.
43 Raftos JE, Whillier S, Kuchel PW: Glutathione synthesis and turnover in the human erythrocyte: alignment of a model based on detailed enzyme kinetics with experimental data. J Biol Chem 2010;285:23557-23567.
44 Ackerman DG, Feigenson GW: Multiscale modeling of four-component lipid mixtures: domain composition, size, alignment, and properties of the phase interface. J Phys Chem B 2015;119:4240-4250.
45 Gu RX, Ingolfsson HI, de Vries AH, Marrink SJ, Tieleman DP: Ganglioside-Lipid and Ganglioside-Protein Interactions Revealed by Coarse-Grained and Atomistic Molecular Dynamics Simulations. J Phys Chem B 2017;121:3262-3275.
46 Koldso H, Shorthouse D, Helie J, Sansom MS: Lipid clustering correlates with membrane curvature as revealed by molecular simulations of complex lipid bilayers. PLoS Comput Biol 2014;10:e1003911.
47 Veatch SL, Keller SL: Seeing spots: complex phase behavior in simple membranes. Biochim Biophys Acta 2005;1746:172-185.
48 Kahya N, Schwille P: Fluorescence correlation studies of lipid domains in model membranes. Mol Membr Biol 2006;23:29-39.
49 Sezgin E, Gutmann T, Buhl T, Dirkx R, Grzybek M, Coskun U, Solimena M, Simons K, Levental I, Schwille P: Adaptive lipid packing and bioactivity in membrane domains. PLoS One 2015;10:e0123930.

50 Chapman D: Phase transitions and fluidity characteristics of lipids and cell membranes. Q Rev Biophys 1975;8:185-235.
51 Garcia-Arribas AB, Alonso A, Goni FM: Cholesterol interactions with ceramide and sphingomyelin. Chem Phys Lipids 2016;199:26-34.
52 Manno S, Takakuwa Y, Mohandas N: Modulation of erythrocyte membrane mechanical function by protein 4.1 phosphorylation. J Biol Chem 2005;280:7581-7587.
53 Glogowska E, Schneider ER, Maksimova Y, Schulz VP, Lezon-Geyda K, Wu J, Radhakrishnan K, Keel SB, Mahoney D, Freidmann AM, Altura RA, Gracheva EO, Bagriantsev SN, Kalfa TA, Gallagher PG: Novel mechanisms of PIEZO1 dysfunction in hereditary xerocytosis. Blood 2017;130:1845-1856.
54 Koshy C, Ziegler C: Structural insights into functional lipid-protein interactions in secondary transporters. Biochim Biophys Acta 2015;1850:476-487.
55 Bhatia T, Cornelius F, Brewer J, Bagatolli LA, Simonsen AC, Ipsen JH, Mouritsen OG: Spatial distribution and activity of Na(+)/K(+)-ATPase in lipid bilayer membranes with phase boundaries. Biochim Biophys Acta 2016;1858:1390-1399.
56 Dawaliby R, Trubbia C, Delporte C, Masureel M, Van Antwerpen P, Kobilka BK, Govaerts C: Allosteric regulation of G protein-coupled receptor activity by phospholipids. Nat Chem Biol 2016;12:35-39.
57 Posada IM, Fantini J, Contreras FX, Barrantes F, Alonso A, Goni FM: A cholesterol recognition motif in human phospholipid scramblase 1. Biophys J 2014;107:1383-1392.
58 Qi Y, Andolfi L, Frattini F, Mayer F, Lazzarino M, Hu J: Membrane stiffening by STOML3 facilitates mechanosensation in sensory neurons. Nat Commun 2015;6:8512-8525.
59 Ridone P, Grage SL, Patkunarajah A, Battle AR, Ulrich AS, Martinac B: "Force-from-lipids" gating of mechanosensitive channels modulated by PUFAs. J Mech Behav Biomed Mater 2018;79:158-167.
60 Saotome K, Murthy SE, Kefauver JM, Whitwam T, Patapoutian A, Ward AB: Structure of the mechanically activated ion channel Piezo1. Nature 2017;554:481-486.
61 Wu J, Lewis AH, Grandl J: Touch, Tension, and Transduction - The Function and Regulation of Piezo Ion Channels. Trends Biochem Sci 2017;42:57-71.
62 Bavi O, Vossoughi M, Naghdabadi R, Jamali Y: The Combined Effect of Hydrophobic Mismatch and Bilayer Local Bending on the Regulation of Mechanosensitive Ion Channels. PLoS One 2016;11:e0150578.
63 Nourse JL, Pathak MM: How cells channel their stress: Interplay between Piezo1 and the cytoskeleton. Semin Cell Dev Biol 2017;71:3-12.
64 Pang Y, Zhu H, Wu P, Chen J: The characterization of plasma membrane Ca2+-ATPase in rich sphingomyelin-cholesterol domains. FEBS Lett 2005;579:2397-2403.
65 Tang D, Dean WL, Borchman D, Paterson CA: The influence of membrane lipid structure on plasma membrane Ca2+ -ATPase activity. Cell Calcium 2006;39:209-216.
66 Liu C, Weng H, Chen L, Yang S, Wang H, Debnath G, Guo X, Wu L, Mohandas N, An X: Impaired intestinal calcium absorption in protein 4.1R-deficient mice due to altered expression of plasma membrane calcium ATPase 1b (PMCA1b). J Biol Chem 2013;288:11407-11415.
67 Di Leva F, Domi T, Fedrizzi L, Lim D, Carafoli E: The plasma membrane Ca2+ ATPase of animal cells: structure, function and regulation. Arch Biochem Biophys 2008;476:65-74.
68 Pignataro MF, Dodes-Traian MM, Gonzalez-Flecha FL, Sica M, Mangialavori IC, Rossi JP: Modulation of plasma membrane Ca2+-ATPase by neutral phospholipids: effect of the micelle-vesicle transition and the bilayer thickness. J Biol Chem 2015;290:6179-6190.
69 Wang YH, Collins A, Guo L, Smith-Dupont KB, Gai F, Svitkina T, Janmey PA: Divalent cation-induced cluster formation by polyphosphoinositides in model membranes. J Am Chem Soc 2012;134:3387-3395.
70 Abe M, Makino A, Hullin-Matsuda F, Kamijo K, Ohno-Iwashita Y, Hanada K, Mizuno H, Miyawaki A, Kobayashi T: A role for sphingomyelin-rich lipid domains in the accumulation of phosphatidylinositol-4, 5-bisphosphate to the cleavage furrow during cytokinesis. Mol Cell Biol 2012;32:1396-1407.
71 Zaidi A, Barron L, Sharov VS, Schoneich C, Michaelis EK, Michaelis ML: Oxidative inactivation of purified plasma membrane Ca2+-ATPase by hydrogen peroxide and protection by calmodulin. Biochemistry 2003;42:12001-12010.
72 Sharp JS, Tomer KB: Analysis of the oxidative damage-induced conformational changes of apo- and holocalmodulin by dose-dependent protein oxidative surface mapping. Biophys J 2007;92:1682-1692.
73 Zaidi A: Plasma membrane Ca-ATPases: Targets of oxidative stress in brain aging and neurodegeneration. World J Biol Chem 2010;1:271-280.
74 Subbaiah PV, Sircar D, Lankalapalli RS, Bittman R: Effect of double bond geometry in sphingosine base on the antioxidant function of sphingomyelin. Arch Biochem Biophys 2009;481:72-79.